Research Article

Selective electroreduction of CO_2 to C_{2+} products on cobalt decorated copper catalysts

Sanaz Soodi[1,2,3,4,#], Jun-Jun Zhang[5,6,#], Jie Zhang[1,2], Yuefeng Liu[7] , Mohsen Lashgari[3,8], Spyridon Zafeiratos[9], Andreas Züttel[1,2], Kun Zhao[1,2,10,*], Wen Luo[5,*]

[1]Laboratory of Materials for Renewable Energy (LMER), Institute of Chemical Sciences and Engineering (ISIC), Basic Science Faculty (SB), École Polytechnique Fédérale de Lausanne (EPFL) Valais/Wallis, Energypolis, Sion CH-1951, Switzerland.
[2]Empa Materials Science & Technology, Dübendorf CH-8600, Switzerland.
[3]Chemistry department, Institute for Advanced Studies in Basic Sciences (IASBS), Zanjan 45137-66731, Iran.
[4]Department of Chemical and Process Engineering, University of Surrey, Guildford GU2 7XH, UK.
[5]School of Environmental and Chemical Engineering, Shanghai University, Shanghai 200444, China.
[6]Department of Chemical Engineering, Sichuan University, Chengdu 610065, Sichuan, China.
[7]Dalian National Laboratory for Clean Energy (DNL), Dalian Institute of Chemical Physics (DICP), Chinese Academy of Science, Dalian 116023, Liaoning, China.
[8]Center for Research in Climate Change and Global Warming: Hydrogen and Solar Division, Zanjan 45137-66731, Iran.
[9]Institute for Chemistry and Energy, Environment and Health processes (ICPEES) - UMR 7515 CNRS - University of Strasbourg, Strasbourg 67087, France.
[10]Department of Chemistry, University of Washington, Seattle, WA 98195-1700, USA.
[#]Authors contributed equally.

[*]**Correspondence to:** Dr. Kun Zhao, Laboratory of Materials for Renewable Energy (LMER), Institute of Chemical Sciences and Engineering (ISIC), Basic Science Faculty (SB), École Polytechnique Fédérale de Lausanne (EPFL) Valais/Wallis, Energypolis, Rue de l'Industrie 17, Sion CH-1951, Switzerland. Email: kzhao20@uw.edu; Prof. Wen Luo, School of Environmental and Chemical Engineering, Shanghai University, 99 Shangda Road, Shanghai 200444, China. E-mail: wenluo@shu.edu.cn

Abstract

Cu-catalyzed electrochemical CO_2 reduction reaction (CO_2RR) to multi-carbon (C_{2+}) products is often plagued by low selectivity because the adsorption energies of different reaction intermediates are in a linear scaling relationship. Development of Cu-based bimetallic catalysts has been considered as an attractive strategy to address this issue; however, conventional bimetallic catalysts often avoid metals with strong CO adsorption energies to prevent surface poisoning. Herein, we demonstrated that limiting the amount of Co in CuCo bimetallic catalysts can enhance C_{2+} product selectivity. Specifically, we synthesized a series of $CuCo_x$ catalysts with trace amounts of Co (0.07-1.8 at%) decorated on the surface of Cu nanowires using a simple dip coating method. Our

results revealed a volcano-shaped correlation between Co loading and C_{2+} selectivity, with the $CuCo_{0.4\%}$ catalyst exhibiting a 2-fold increase in C_{2+} selectivity compared to the Cu nanowire sample. *In situ* Raman and Infrared spectroscopies suggested that an optimal amount of Co could stabilize the Cu oxide/hydroxide species under the CO_2RR condition and promote the adsorption of CO, thus enhancing the C_{2+} selectivity. This work expands the potential for developing Cu-based bimetallic catalysts for CO_2RR.

Keywords: Electrochemical CO_2 reduction, copper cobalt catalyst, multi-carbon products, reaction mechanism, *in situ* techniques

INTRODUCTION

Electrochemical reduction of CO_2 (CO_2RR) under ambient conditions is a promising approach to mitigate the increasing concentration of CO_2 in the atmosphere and produce high value-added products.[1] Cu-based materials have been extensively studied as catalysts for CO_2RR, as Cu is reported to be the only metal that can reduce CO_2 to various multi-carbon (C_{2+}) products, including gaseous hydrocarbons (e.g., C_2H_4 and C_2H_6) and liquid oxygenates (e.g., ethanol and propanol).[2-9] However, the selectivity of C_{2+} on pure Cu is poor because the competing reactions, such as hydrogen evolution (HER) and CO_2-to-C_1 (e.g., CO and HCOOH) reactions, require similar (or even lower) overpotentials compared to those for CO_2-to-C_{2+} reactions.

To date, various strategies have been applied to improve the selectivity of C_{2+} over Cu-based catalysts, including tuning the exposed facets[10], adjusting the oxidation state[11], introducing defects[12], and engineering the electrode structure[13] and hydrophobicity[14]. Among them, introducing a second metal to Cu has attracted great attention[6,15]. For instance, recent studies of Cu-Au,[16] Cu-Ag,[7] and Cu-Zn[17] catalysts have shown enhanced selectivity towards C_{2+} products. Notably, in these cases, the second metals (i.e., Au, Ag and Zn) are intrinsically selective for electrochemically reducing CO_2 to CO due to their weak binding strength with CO. Therefore, these metals can serve as a CO reservoir to enhance the *CO coverage on Cu surface, thus increasing the C–C coupling probability[1]. In contrast, many other metals, such as Fe, Ni, Co, *etc.*, are intrinsically not selective for CO_2RR because CO can strongly adsorb on these metals, leading to the poisoning of the catalyst surface and the high H_2 selectivity. Thus, most researchers have tried to remove these metals during the sample and electrolyte preparation[18]. Interestingly, recent attempts have shown that Ni-Cu and Co-Cu alloys can also be active for CO_2RR. However, the selectivity of these catalysts varies for products such as CO, HCOOH, and C_2H_4, and the enhanced catalytic activity is believed to result from adjustments in the d-band structure, size effects, and/or additional binding sites[19-21]. Thus, further investigations are necessary to improve the design of such bimetallic catalysts. Building upon prior findings, we hypothesize that by strategically incorporating Group VIII metals (e.g., Co) onto the Cu surface and precisely adjusting their atomic ratios, it is possible to optimize the surface state of Cu and enhance the adsorption strength of *CO, ultimately improving selectivity for C_{2+} products.

Therefore, this work successfully designed and synthesized Cu nanowires (NWs) decorated with trace amounts of Co ($CuCo_x$, x = 0.07%, 0.4%, and 1.8%) as advanced electrocatalysts for CO_2RR. A simple dip coating method developed in our previous studies was applied to ensure that Co was deposited on the surface of Cu and avoid contamination by surfactants[22]. We found that with an optimal loading of Co (i.e., $CuCo_{0.4\%}$), the C_{2+} selectivity was doubled than that of pure Cu, reaching > 40% faradaic efficiency (FE) at -1.0 V *vs.* reversible hydrogen electrode (RHE). *In situ* Raman and attenuated total reflectance-surface-enhanced infrared absorption spectroscopy (ATR-SEIRAS) revealed that the mixed Cu oxide states stabilized by Co could enhance the adsorption of *CO intermediates and consequently promote the C_{2+} selectivity.

EXPERIMENTAL

$CuCo_x$ (x = 0.07%, 0.4%, and 1.8%) catalysts were prepared using a simple dip coating method (Experimental details in Supplementary Materials). Briefly, a piece of Cu foil was first immersed in a mixed solution of NaOH and $(NH_4)_2S_2O_8$ for 10 min to chemically oxidize its surface layers to grow $Cu(OH)_2$ NWs. This sample is named Cu NWs in the remainder of the paper to simplify the notation. The $CuCo_x$ samples were produced via immersing these Cu NWs in aqueous $Co(NO_3)_2$ solution for 30 s to adsorb cobalt species, followed by heat treatment at 150 °C and electrochemical reduction under CO_2RR condition (i.e., -0.8 V *vs.* RHE in 0.1 M $KHCO_3$ for 20 min) [Figure 1A][22]. The atomic ratio of Co:Cu of the $CuCo_x$ samples was tuned by changing the concentration of the $Co(NO_3)_2$ solution from 2 to 50 mM.

RESULTS AND DISCUSSION

The morphology of the Cu NWs and $CuCo_x$ samples was studied using a scanning electron microscope (SEM) [Supplementary Figure 1]. Well-defined NW structure with an average length of ~10 μm and width of ~200 nm is observed [Figure 1B]. Notably, the NW morphology of the Cu sample did not change after Co deposition. This can be ascribed to the low concentration of the $Co(NO_3)_2$ solution and the short dipping time [Supplementary Figure 1]. The X-ray diffraction patterns (XRD) of $CuCo_x$ samples were the same as those of the Cu NWs sample, with high-intensity diffraction peaks from metallic Cu [Figure 1C]. This indicates metallic Cu dominates the composition in the Cu NWs and $CuCo_x$ samples. Characteristic diffraction peaks of Co-related crystal phases were not observed. This can be attributed to the low loading of Co as well.

We further examined the surface compositions of the Cu NWs and $CuCo_x$ samples using X-ray photoelectron spectroscopy (XPS) analysis after each sample preparation step. In the case of the Cu NW sample, Cu stayed in $Cu(OH)_2$ form (not shown). As shown in Figure 1D, Cu remained as $Cu(OH)_2$ with Cu 2p peaks at 934.7 and 954.6 eV after Co deposition. It turned to the form of CuO after the heat treatment due to dehydration. After pre-electrochemical reduction treatment, the Cu 2p peak shifted to a lower binding energy and the satellite peaks disappeared, indicating that CuO was reduced to Cu^0/Cu^{1+} species[23,24]. Importantly, Co 2p peaks were found in the XPS, although with low intensities [Supplementary Figure 2], demonstrating the successful decoration of Co on Cu NWs.

To gain detailed information of the microstructure and the elemental distribution, high-angle annular dark-field scanning transmission electron microscopy (HAADF-STEM) and energy dispersive X-ray spectroscopy (EDX) measurements were performed. As shown in Figure 1E, the STEM-coupled EDX mapping further corroborates the successful deposition of Co on Cu NWs. Notably, Co species are highly dispersed, as observed from the high-resolution transmission electron microscopy (TEM) images and the EDX mapping. Selected area electron diffraction (SAED) analysis was then conducted to investigate the crystal structure of the NWs [Supplementary Figure 3]. Only metallic Cu diffraction rings were observed. This proved that the NWs are metallic Cu-dominated, although the surfaces were oxidized. The SAED analysis and the XRD results demonstrate that the Cu species mainly consists of crystalline Cu both in the NWs and the Cu foils of the Cu NWs and $CuCo_x$ samples. In addition, all studied samples showed the same diffraction ring, suggesting that the bulk crystal structure did not change noticeably from the Cu NWs to $CuCo_x$ samples with varying amounts of Co deposited. No Co diffractions were observed in SAED, consistent with the XRD results, further implying that no long-range ordered cobalt species were present. This can be due to the low loading and high dispersion of Co.

Next, we performed electrochemical OH adsorption to study the influence of Co on the surface structure of the $CuCo_x$ samples. In cyclic voltammograms (CVs), OH adsorption peaks exhibited distinctly at various
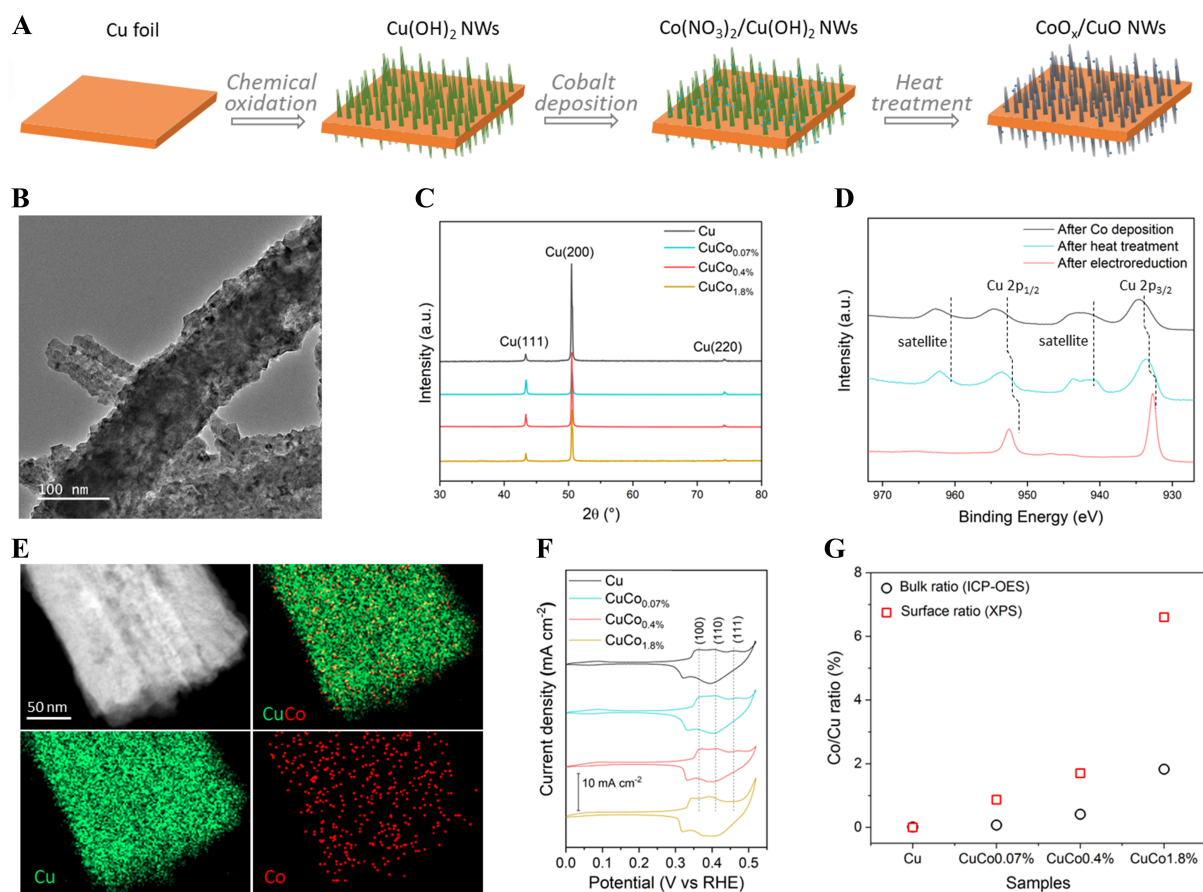
Figure 1. (A) Schematic illustration for synthesizing CoO_x/CuO NWs; samples after electroreduction during CO_2RR are denoted as $CuCo_x$ catalysts; (B) Representative TEM image of the $CuCo_{0.4\%}$ sample; (C) XRD of Cu and $CuCo_x$ catalysts; (D) Cu 2p XPS spectra of $CuCo_{0.4\%}$ after Co deposition, heat treatment, and electroreduction; (E) Element maps the $CuCo_{0.4\%}$ sample; (F) Cyclic voltammograms recorded in N_2 purged 1.0 M KOH capturing the surface-specific adsorption of oxygen (OH); (G) Bulk and surface atomic ratios of Co:Cu for Cu and $CuCo_x$ catalysts obtained using ICP-OES and XPS, respectively. NWs: Nanowires; CO_2RR: CO_2 reduction reaction; TEM: transmission electron microscopy; XRD: X-ray diffraction patterns; XPS: X-ray photoelectron spectroscopy; ICP-OES: inductively coupled plasma optical emission spectrometry.

potentials on distinct facets of Cu crystals, thus allowing the probing of surface structure of Cu[25,26]. As shown in Figure 1F, three OH desorption peaks assigned to Cu (111), (110), and (100) facets were observed for the Cu NWs and $CuCo_x$ samples. These peaks are almost identical for the Cu, $CuCo_{0.07\%}$, and $CuCo_{0.4\%}$ samples. However, the peak positions were shifted to ~0.02 V lower for the $CuCo_{1.8\%}$ sample, indicating a weaker binding of OH on this sample surface. Intriguingly, the (111) peak for $CuCo_{1.8\%}$ almost diminished, indicating that the surface structure of Cu was only affected by a high loading of Co. To conclude, using a simple dip coating method, a series of $CuCo_x$ catalysts with highly dispersed Co decorated on the surface of Cu NWs were successfully synthesized. In addition, the Co:Cu ratio in the catalyst was quantitatively analyzed by XPS and inductively coupled plasma optical emission spectrometry (ICP-OES). Quantitative determination of the surface Co:Cu ratio from the XPS analysis showed a fast increase from $CuCo_{0.07\%}$ to $CuCo_{1.8\%}$. Interestingly, when compared with the bulk Co:Cu ratio measured with the ICP-OES, the Co concentration on the surface is much higher than that in the bulk of the $CuCo_x$ samples [Figure 1G]. This is similar to our previous findings, which show that the dip coating method allows the deposition of metal species to concentrate on the surface of the NWs[22].

The CO_2RR activity and product distribution from Cu NWs and $CuCo_x$ samples were evaluated in CO_2-saturated 0.1 M $KHCO_3$ electrolyte within a two-compartment H-cell. The geometric current densities in the potential range of -0.6 to -1.2 V *vs.* RHE are shown in Figure 2. Cu and $CuCo_x$ catalysts show very similar geometric current densities in the entire potential range [Figure 2A]. This could be attributed to their similar morphology and almost identical electrochemical active surface area (ECSA) [Supplementary Figure 4], as SEM results showed that the Cu NW structure was well preserved after Co deposition [Supplementary Figure 1].

To assess the influence of Co on the catalytic selectivity, gas and liquid products were analyzed using gas chromatography (GC) and ^1H nuclear magnetic resonance (NMR), respectively. The FEs of the reaction products are presented in Figure 2B and C and Supplementary Figure 4. Since Co is known to be more active than Cu towards HER, high loading of Co (i.e., $CuCo_{1.8}$ with 6.6 at% coverage of surface Co, as shown in Figure 1G) enhances HER performance unsurprisingly compared to Cu NWs. However, $CuCo_{0.07\%}$ and $CuCo_{0.4\%}$ show similar H_2 selectivity in the low overpotential range (-0.6 to -0.9 V *vs.* RHE) and 10%-20% lower H_2 selectivity at higher overpotentials (-1.0 to -1.2 V *vs.* RHE) [Supplementary Figure 5] compared to Cu NWs. The reduction products of CO_2 were influenced more dramatically due to the decoration of Co. As shown in Figure 2B and C, the CO FEs of all three $CuCo_x$ samples were significantly lower than those of the Cu NWs, and C_{2+} FEs of these $CuCo_x$ samples were significantly higher than those of the Cu NWs. Specifically, the highest FE for C_{2+} increased sharply from 19.5% for Cu to 33.2% for $CuCo_{0.07\%}$, 40.7% for $CuCo_{0.4\%}$, and 26.0% for $CuCo_{1.8\%}$. CO is widely accepted as the key reaction intermediate for converting CO_2 to C_{2+} on Cu. The fast decrease of CO detected by GC in Figure 2B can be ascribed to the accelerated consumption of the adsorbed *CO on the surface in forming C_{2+}, resulting in decreased desorbed CO. The above results suggest that Co plays an important role in lowering gaseous CO release and facilitating C_{2+} production. Meanwhile, the suppressed H_2 production on $CuCo_x$ samples compared to Cu NWs could also contribute to the more effective C_{2+} production, as more electrons were consumed by C–C coupling instead of HER.

Intriguingly, the selectivity of C_{2+} products increases with Co loading until 0.4 at%, but then decreases with further Co loading (1.8 at%) [Figure 2C]. To verify this trend, we prepared two additional Co-modified Cu catalysts with 0.2% ($CuCo_{0.2\%}$) and 1.1% Co ($CuCo_{1.1\%}$) and tested their CO_2RR performance under identical conditions. As shown in Figure 2D, the FEs for C_2H_4 and C_2H_5OH of the Cu and $CuCo_x$ samples obtained at -1.0 V *vs.* RHE demonstrate a volcano-shape dependence on the Co loading, where the $CuCo_{0.4\%}$ catalyst displays the highest FE for both C_2H_4 (27.3%) and C_2H_5OH (10.7%) productions. This performance surpasses that of the state-of-the-art CuCo catalysts currently reported in the literature [Supplementary Table 1]. As the morphology and the ECSA of the Cu NWs and $CuCO_x$ samples are very similar, the influence of the local reaction environment can thus be ruled out. Therefore, these results demonstrate that an optimal loading of Co could effectively improve the selectivity of Cu towards C_{2+} products by suppressing the H_2 evolution and accelerating C–C coupling, which is consistent with previous research[21,27].

To understand the enhanced selectivity towards C_{2+} products on $CuCo_x$ catalysts, *in situ* surface-enhanced Raman spectroscopy (SERS) was employed to probe the adsorbed intermediates on the catalyst surfaces[2,28]. The NW structure of the Cu and $CuCo_x$ catalysts was reported to enhance Raman signals; thus, additional surface manipulation was not required[29,30]. We first examined the surface of $CuCo_{0.4\%}$ as it showed the highest performance of C_{2+} production. Figure 3A shows the potential-dependent SERS spectra of $CuCo_{0.4\%}$ acquired in CO_2-saturated 0.1 M $KHCO_3$ electrolyte at different applied potentials. At open circuit potential (OCP), the $CuCo_{0.4\%}$ samples exhibited three characteristic Raman bands of CuO at around ~300, ~350, and ~590 cm^{-1}[31]. These peaks disappeared after applying a reduction potential of -0.4 V *vs.* RHE, demonstrating
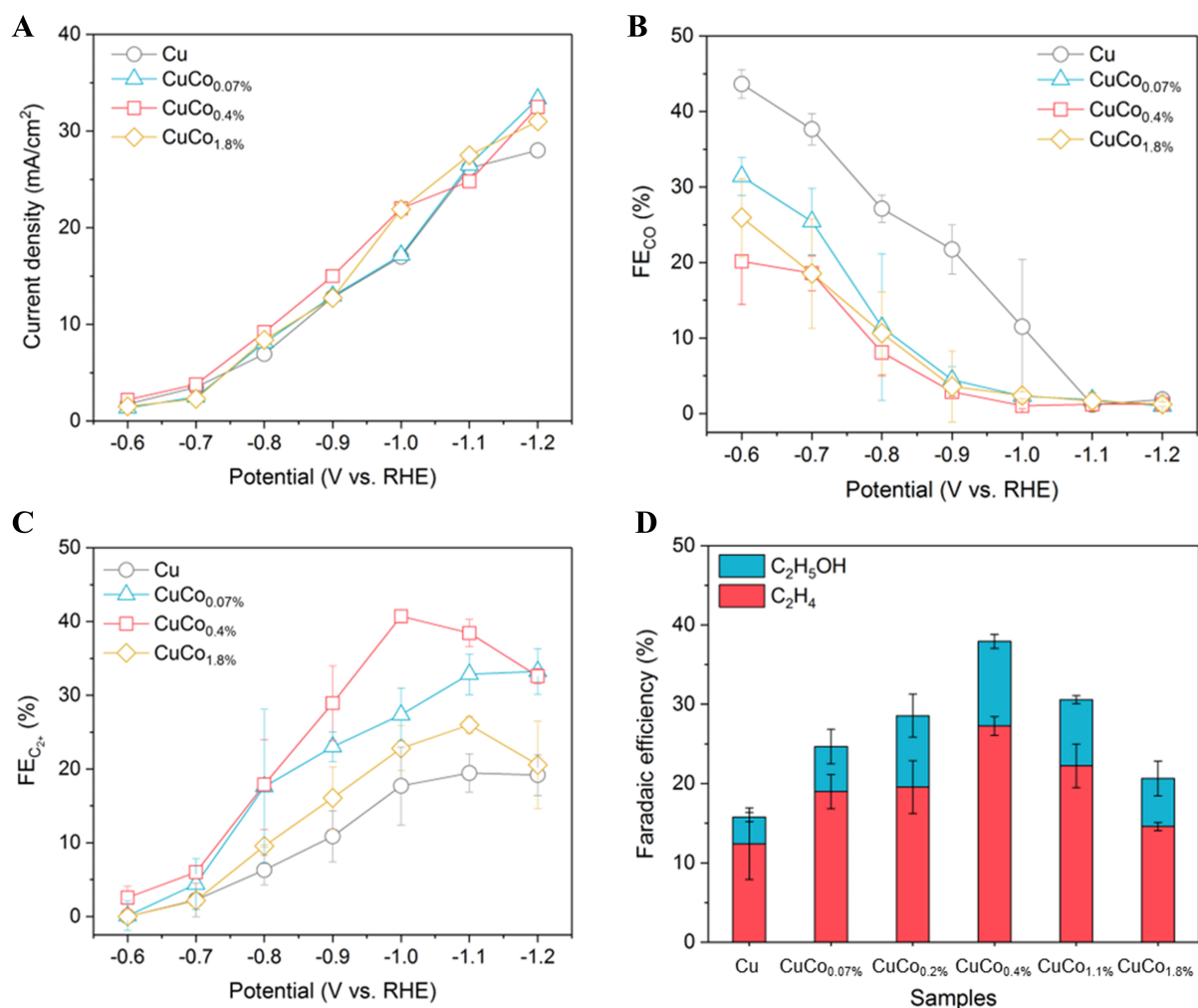
Figure 2. (A) Current density, (B) Faradaic efficiency of CO, and (C) Faradaic efficiency of C_{2+} for Cu, $CuCo_{0.07\%}$, $CuCo_{0.4\%}$ and $CuCo_{1.8\%}$; (D) Faradaic efficiency of C_2H_4 and C_2H_5OH for CuCo samples with different amounts of Co. Error bars are means $\pm$ SD ($n = 3$ replicates). C_{2+}: Multi-carbon.

that the CuO in bulk can be reduced promptly at potentials more negative than -0.4 V *vs.* RHE, which agrees with our XRD and SAED analysis. However, two weak bands at ~490 and ~570 cm^{-1} attributable to the surface Cu oxide/hydroxide species [e.g., a mixture of CuO_x and $Cu(OH)_y$], named as $CuO_x/(OH)_y$, are present after reduction[29,32,33]. These oxidized Cu species could be attributed to the dynamic oxidation of the Cu surface and the adsorption of -OH groups during the CO_2RR and HER processes[29,32]. In addition, three Raman bands related to $^*CO$ can be observed in the potential range of -0.6 to -0.8 V *vs.* RHE: the two low-frequency bands at ~280 and ~360 cm^{-1} can be assigned to the frustrated rotation and stretching vibration of Cu-CO, respectively; and the high-frequency broad band located between 1,950 and 2,100 cm^{-1} is caused by intramolecular $C\equiv O$ stretching vibrations with various binding configurations[30,34]. Both the surface Cu oxide species and the $^*CO$-related intermediates disappeared after removing the applied potential, indicating that these species are generated and stabilized under the CO_2RR condition[35].

To explore the influence of Co deposition on the CO_2RR process, SERS was also employed to probe the surface speciation of Cu, $CuCo_{0.07\%}$, and $CuCo_{1.8\%}$ samples. As shown in Figure 3B, all four samples share similar spectral features at a reduction potential of -0.8 V, suggesting the presence of similar surface species.
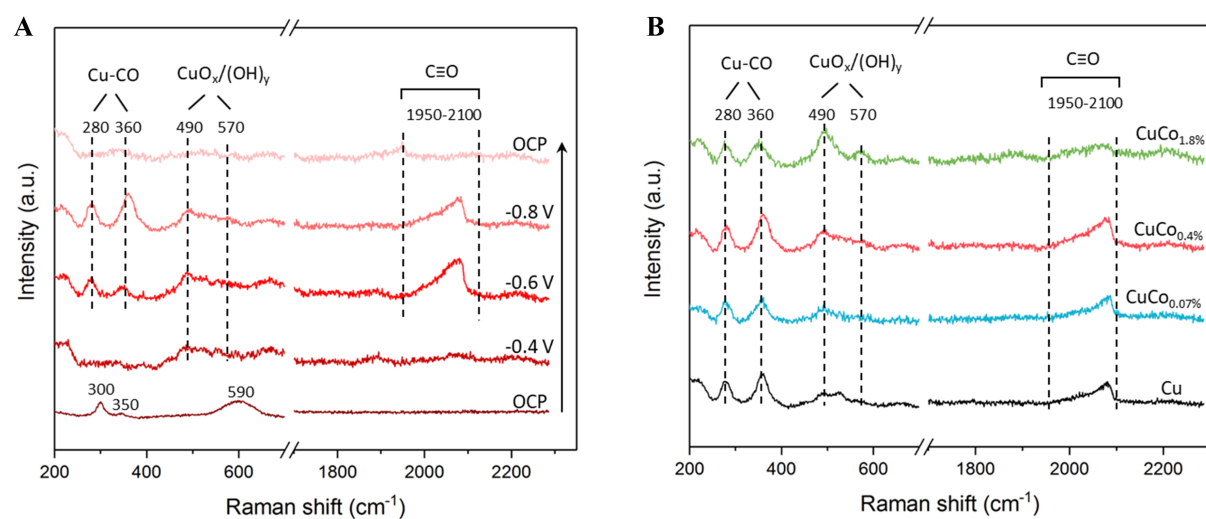
Figure 3. *In situ* Raman spectra of (A) $CuCo_{0.4\%}$ at different applied potentials; and (B) various $CuCo_x$ samples at -0.8 V *vs.* RHE in CO_2 saturated 0.1 M $KHCO_3$. RHE: Reversible hydrogen electrode.

However, the relative intensities of these peaks differ [Supplementary Figure 6]. While the peak intensity of $CuO_x/(OH)_y$ increases with Co deposition amount, the Cu-CO and C≡O peak intensities are maximized for the $CuCo_{0.4\%}$ sample. The trend for $CuO_x/(OH)_y$ peak intensity agrees with previous studies that showed that isolated Co atoms could stabilize the Cu_2O surface by increasing the activation barrier of surface oxygen abstraction[36]. The trend for Cu-CO and C≡O peak intensities are in line with the C_{2+} selectivity observed in Figure 2C, indicating that high *CO coverage is the obvious reason for C–C coupling, therein, a higher C_{2+} production[7,13]. Various studies have shown that mixed oxide states of Cu could enhance the CO_2-to-C_{2+} conversion[11,37-39]. For instance, by using density functional theory (DFT) calculations and *in situ* SEIRAS, Zhang *et al.* demonstrated that the $Cu^{\delta+}$ site at the $Cu^0/Cu^{\delta+}$ interface favors the formation of *CHO intermediates, which can subsequently couple with *CO on adjacent Cu^0 surfaces to form *OCCHO intermediates, promoting the generation of C_{2+} products[40]. In our case, we anticipate that the $CuCo_{0.4\%}$ sample shows higher C_{2+} selectivity than the other samples due to the coexistence of Cu^0 and $Cu^{\delta+}$ species in an optimized ratio.

Notably, due to the low loading of Co, we could not detect any vibrational bands associated with Co species or reaction intermediates adsorbed on Co. However, the role of Co species in tuning the reaction pathway should not be ignored since the binding of *CO and *H to the Co surface is much stronger than that to the Cu surface, which can certainly affect the reaction pathways[41,42]. Further, a recent study shows that in CuCo single atom alloys, Cu sites neighboring Co atomic sites could accelerate CO_2-to-CO conversion and Cu-Co sites also favor the deoxygenation of *HOCCH, which increases the selectivity toward ethylene over ethanol[43]. More recently, Luo *et al.* found that Co in cobalt phthalocyanine could promote the C_2 selectivity of Cu catalysts because the adsorption of CO_2, CO, and CO_2RR intermediates could be enhanced on both Co and Cu sites[44]. These results indicate that using strong CO-binding elements to promote the C_{2+} selectivity of Cu is effective, and further mechanism understanding is also required.

To further investigate the formation mechanism of C_{2+} products on the $CuCo_x$ catalysts, *in situ* ATR-SEIRAS was performed over the Cu and $CuCo_{0.4\%}$ catalysts. Figure 4A shows almost no characteristic peak of *CO species detected on the surface of the Cu NWs electrode during the electrocatalytic process. However, on the $CuCo_{0.4\%}$ sample [Figure 4B], a peak appears at a wavelength of 2,080 cm^{-1} from -0.4 V *vs.* RHE and
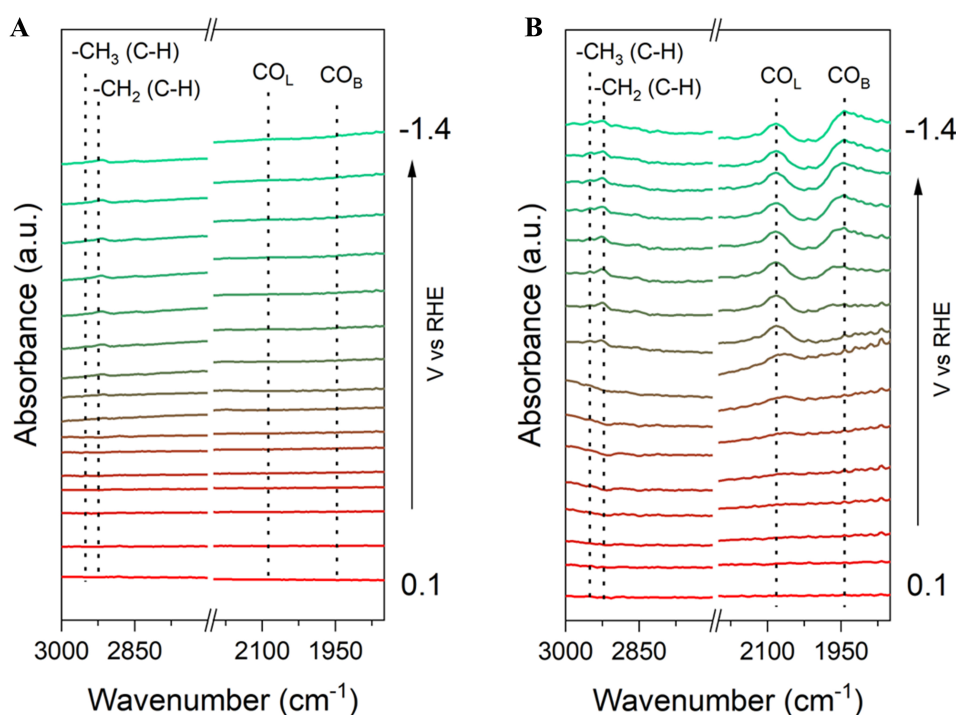
Figure 4. Potential-dependent ATR-SEIRAS spectra for (A) Cu and (B) CuCo$_{0.4\%}$ at 0.1 to -1.4 V *vs.* RHE in CO$_2$-saturated 0.1 M KHCO$_3$. The spectrum taken at 0.2 V *vs.* RHE was used as the reference. ATR-SEIRAS: Attenuated total reflectance-surface-enhanced infrared absorption spectroscopy; RHE: reversible hydrogen electrode.

another at 1,950 cm^{-1} from -0.8 V *vs.* RHE. These peaks can be assigned to the adsorbed *CO species, with the first one belonging to linear adsorption (*CO$_L$) and the second one to bridge adsorption (*CO$_B$), respectively[45]. Further, two additional peaks appear at 2,952 and 2,923 cm^{-1} for both Cu NWs and CuCo$_{0.4\%}$ samples with relatively low intensities, attributed to the C-H extension of methyl (-CH$_3$) and methylene (-CH$_2$), respectively, in agreement with the observed CH$_3$CH$_2$OH production on these catalysts[46]. Overall, the *in situ* ATR-SEIRAS results indicate a higher *CO coverage on the CuCo$_{0.4\%}$ surface than the Cu NWs surface, and the reason could be the higher *CO adsorption energy on CuCo surfaces than pure Cu surfaces. Consequently, the high *CO coverage could facilitate the formation of C$_{2+}$ products on the CuCo$_{0.4\%}$ sample[4]. Consistent with the *in situ* Raman results, the optimal adsorption of *CO species and subsequent C–C coupling can be attributed to the synergistic effect between Cu and Co metals and the coexistence of reduced and oxidized Cu species.

CONCLUSIONS

In summary, this work shows that Co, despite being a non-CO$_2$RR selective metal, can be used to decorate the Cu surface to improve the selectivity towards C$_{2+}$ products. With an optimized amount of Co, the CuCo$_{0.4\%}$ sample showed 40.7% FE for C$_{2+}$ at -1.0 V *vs.* RHE, two times higher than that of the Cu sample (19.5%). *Ex situ* techniques indicated that with a low deposition amount of Co, the crystal structure and morphology of Cu NWs were not influenced. However, *in situ* Raman spectra revealed that Co could stabilize the Cu$^{\delta+}$ species on the CuCo$_x$ surface, and *in situ* infrared spectroscopy indirectly proves that coexistence of Co, Cu^0 and Cu$^{\delta+}$ may promote the adsorption of *CO, thus accelerating the C–C coupling. We believe this study can inspire the development of other Cu-based bimetallic catalysts for CO$_2$RR.

DECLARATIONS

Authors' contributions

Conceptualized and supervised the project: Luo W, Zhao K, Züttel A

Synthesized the catalysts and performed the electrochemical tests: Soodi S

Performed the *in situ* analysis: Zhang JJ

Performed sample characterizations and data analysis: Zhang J, Liu Y, Luo W

Co-wrote the manuscript: Soodi S, Zhang JJ, Zhao K, Luo W

Reviewed the paper: Lashgari M, Zafeiratos S, Züttel A

All the authors discussed the results and revised the manuscript.

Availability of data and materials

The data that support the findings of this study are available from the corresponding author upon reasonable request.

Conflicts of interest

Liu Y is the Guest Editor of the Special Issue "Carbon in Catalysis" of the Journal of *Chemical Synthesis*, while the other authors have declared that they have no conflicts of interest.

Ethical approval and consent to participate

Not applicable.

Consent for publication

Not applicable.

REFERENCES

1. De Luna P, Hahn C, Higgins D, Jaffer SA, Jaramillo TF, Sargent EH. What would it take for renewably powered electrosynthesis to displace petrochemical processes? *Science* 2019;364:eaav3506. DOI PubMed
2. Pham THM, Zhang J, Li M, et al. Enhanced electrocatalytic CO_2 reduction to C_{2+} products by adjusting the local reaction environment with polymer binders. *Adv Energy Mater* 2022;12:2103663. DOI
3. Zhang J, Luo W, Züttel A. Crossover of liquid products from electrochemical CO_2 reduction through gas diffusion electrode and anion exchange membrane. *J Catal* 2020;385:140-5. DOI
4. Zhang J, Luo W, Züttel A. Self-supported copper-based gas diffusion electrodes for CO_2 electrochemical reduction. *J Mater Chem A* 2019;7:26285-92. DOI
5. Koolen CD, Luo W, Züttel A. From single crystal to single atom catalysts: structural factors influencing the performance of metal catalysts for CO_2 electroreduction. *ACS Catal* 2023;13:948-73. DOI
6. Koolen CD, Oveisi E, Zhang J, et al. Low-temperature non-equilibrium synthesis of anisotropic multimetallic nanosurface alloys for electrochemical CO_2 reduction. *Nat Synth* 2024;3:47-57. DOI
7. Zhang J, Pham THM, Ko Y, et al. Tandem effect of Ag@C@Cu catalysts enhances ethanol selectivity for electrochemical CO_2 reduction in flow reactors. *Cell Rep Phys Sci* 2022;3:100949. DOI
8. Zhang J, My Pham TH, Gao Z, et al. Electrochemical CO_2 reduction over copper phthalocyanine derived catalysts with enhanced selectivity for multicarbon products. *ACS Catal* 2023;13:9326-35. DOI
9. Gao Y, Xiao H, Ma X, et al. Cooperative adsorption of interfacial Ga-N dual-site in GaOOH@N-doped carbon nanotubes for enhanced electrocatalytic reduction of carbon dioxide. *J Colloid Interface Sci* 2024;654:339-47. DOI PubMed
10. Zhong D, Zhao ZJ, Zhao Q, et al. Coupling of Cu(100) and (110) facets promotes carbon dioxide conversion to hydrocarbons and alcohols. *Angew Chem Int Ed Engl* 2021;60:4879-85. DOI PubMed

11. Yang PP, Zhang XL, Gao FY, et al. Protecting copper oxidation state via intermediate confinement for selective CO_2 electroreduction to C_{2+} fuels. *J Am Chem Soc* 2020;142:6400-8. DOI PubMed

12. Tang C, Shi J, Bai X, et al. CO_2 reduction on copper's twin boundary. *ACS Catal* 2020;10:2026-32. DOI

13. Zhang T, Bui JC, Li Z, Bell AT, Weber AZ, Wu J. Highly selective and productive reduction of carbon dioxide to multicarbon products via in situ CO management using segmented tandem electrodes. *Nat Catal* 2022;5:202-11. DOI

14. García de Arquer FP, Dinh CT, Ozden A, et al. CO_2 electrolysis to multicarbon products at activities greater than 1 A cm^{-2}. *Science* 2020;367:661-6. DOI PubMed

15. Zhou F, Zhang J, Zhang Y, Wu Y, Wang Y, Luo W. Palladium-copper bimetallic catalysts for electroreduction of CO_2 and nitrogenous species. *Coord Chem Rev* 2024;509:215802. DOI

16. Morales-guio CG, Cave ER, Nitopi SA, et al. Improved CO_2 reduction activity towards C_{2+} alcohols on a tandem gold on copper electrocatalyst. *Nat Catal* 2018;1:764-71. DOI

17. Ren D, Gao J, Pan L, et al. Atomic layer deposition of ZnO on CuO enables selective and efficient electroreduction of carbon dioxide to liquid fuels. *Angew Chem* 2019;131:15178-82. DOI

18. Hori Y, Murata A, Takahashi R. Formation of hydrocarbons in the electrochemical reduction of carbon dioxide at a copper electrode in aqueous solution. *J Chem Soc Faraday Trans 1* 1989;85:2309-26. DOI

19. Xu C, Vasileff A, Jin B, et al. Graphene-encapsulated nickel-copper bimetallic nanoparticle catalysts for electrochemical reduction of CO_2 to CO. *Chem Commun* 2020;56:11275-8. DOI PubMed

20. Yan Y, Zhao Z, Zhao J, Tang W, Huang W, Lee J. Atomic-thin hexagonal CuCo nanocrystals with d-band tuning for CO_2 reduction. *J Mater Chem A* 2021;9:7496-502. DOI

21. Bernal M, Bagger A, Scholten F, et al. CO_2 electroreduction on copper-cobalt nanoparticles: size and composition effect. *Nano Energy* 2018;53:27-36. DOI

22. Luo W, Xie W, Mutschler R, et al. Selective and stable electroreduction of CO_2 to CO at the copper/indium interface. *ACS Catal* 2018;8:6571-81. DOI

23. Li M, My Pham TH, Ko Y, et al. Support-dependent Cu–In bimetallic catalysts for tailoring the activity of reverse water gas shift reaction. *ACS Sustain Chem Eng* 2022;10:1524-35. DOI

24. Li M, Luo W, Züttel A. Near ambient-pressure X-ray photoelectron spectroscopy study of CO_2 activation and hydrogenation on indium/copper surface. *J Catal* 2021;395:315-24. DOI

25. Raciti D, Cao L, Livi KJT, et al. Low-overpotential electroreduction of carbon monoxide using copper nanowires. *ACS Catal* 2017;7:4467-72. DOI

26. Wang Y, Raciti D, Wang C. High-flux CO reduction enabled by three-dimensional nanostructured copper electrodes. *ACS Catal* 2018;8:5657-63. DOI

27. Grote J, Zeradjanin AR, Cherevko S, et al. Screening of material libraries for electrochemical CO_2 reduction catalysts - Improving selectivity of Cu by mixing with Co. *J Catal* 2016;343:248-56. DOI

28. Luo W, Zhang Q, Zhang J, Moioli E, Zhao K, Züttel A. Electrochemical reconstruction of ZnO for selective reduction of CO_2 to CO. *Appl Catal B Environ* 2020;273:119060. DOI

29. Zhao Y, Chang X, Malkani AS, et al. Speciation of Cu surfaces during the electrochemical CO reduction reaction. *J Am Chem Soc* 2020;142:9735-43. DOI PubMed

30. Jiang S, Klingan K, Pasquini C, Dau H. New aspects of operando Raman spectroscopy applied to electrochemical CO_2 reduction on Cu foams. *J Chem Phys* 2019;150:041718. DOI PubMed

31. Deng Y, Handoko AD, Du Y, Xi S, Yeo BS. *In Situ* Raman spectroscopy of copper and copper oxide surfaces during electrochemical oxygen evolution reaction: identification of Cu^{III} oxides as catalytically active species. *ACS Catal* 2016;6:2473-81. DOI

32. Moradzaman M, Mul G. In Situ Raman study of potential-dependent surface adsorbed carbonate, CO, OH, and C species on Cu electrodes during electrochemical reduction of CO_2. *ChemElectroChem* 2021;8:1478-85. DOI

33. Liu C, Gong J, Li J, et al. Preanodized Cu surface for selective CO_2 electroreduction to C_1 or C_{2+} products. *ACS Appl Mater Interfaces* 2022;14:20953-61. DOI PubMed

34. Li YC, Wang Z, Yuan T, et al. Binding site diversity promotes CO_2 electroreduction to ethanol. *J Am Chem Soc* 2019;141:8584-91. DOI PubMed

35. Lei Q, Huang L, Yin J, et al. Structural evolution and strain generation of derived-Cu catalysts during CO_2 electroreduction. *Nat Commun* 2022;13:4857. DOI PubMed PMC

36. Wang C, Kong Y, Soldemo M, et al. Stabilization of Cu_2O through site-selective formation of a Co_1Cu hybrid single-atom catalyst. *Chem Mater* 2022;34:2313-20. DOI

37. Chou TC, Chang CC, Yu HL, et al. Controlling the oxidation state of the Cu electrode and reaction intermediates for electrochemical CO_2 reduction to ethylene. *J Am Chem Soc* 2020;142:2857-67. DOI PubMed

38. Lee SY, Jung H, Kim NK, Oh HS, Min BK, Hwang YJ. Mixed copper states in anodized Cu electrocatalyst for stable and selective ethylene production from CO_2 reduction. *J Am Chem Soc* 2018;140:8681-9. DOI PubMed

39. Lei Q, Zhu H, Song K, et al. Investigating the origin of enhanced C_{2+} selectivity in oxide-/hydroxide-derived copper electrodes during CO_2 electroreduction. *J Am Chem Soc* 2020;142:4213-22. DOI PubMed

40. Zhang XY, Lou ZX, Chen J, et al. Direct OC-CHO coupling towards highly C_{2+} products selective electroreduction over stable Cu^0/Cu^{2+} interface. *Nat Commun* 2023;14:7681. DOI PubMed PMC

41. Li J, Xu A, Li F, et al. Enhanced multi-carbon alcohol electroproduction from CO via modulated hydrogen adsorption. *Nat Commun* 2020;11:3685. DOI PubMed PMC

42. Li J, Wang Z, Mccallum C, et al. Constraining CO coverage on copper promotes high-efficiency ethylene electroproduction. *Nat Catal* 2019;2:1124-31. DOI

43. Kim B, Tan YC, Ryu Y, et al. Trace-level cobalt dopants enhance CO_2 electroreduction and ethylene formation on copper. *ACS Energy Lett* 2023;8:3356-64. DOI

44. Luo Y, Yang J, Qin J, et al. Cobalt phthalocyanine promoted copper catalysts toward enhanced electro reduction of CO_2 to C_2: synergistic catalysis or tandem catalysis? *J Energy Chem* 2024;92:499-507. DOI

45. Jiang T, Qin X, Ye K, et al. An interactive study of catalyst and mechanism for electrochemical CO_2 reduction to formate on Pd surfaces. *Appl Catal B Environ* 2023;334:122815. DOI

46. Yan W, Li G, Cui S, et al. Ga-modification near-surface composition of Pt-Ga/C catalyst facilitates high-efficiency electrochemical ethanol oxidation through a C2 intermediate. *J Am Chem Soc* 2023;145:17220-31. DOI PubMed